Damage Localization in a Steel Truss Bridge Using Influence Lines Identified from Vehicle-Induced Acceleration

Published Version:
Quqa, S., Landi, L. (2023). Damage Localization in a Steel Truss Bridge Using Influence Lines Identified from Vehicle-Induced Acceleration. JOURNAL OF BRIDGE ENGINEERING, 28(4), 1-10 [10.1061/JBENF2.BEENG-5978].

Availability:
This version is available at: https://hdl.handle.net/11585/915647 since: 2023-03-22

Published:
DOI: http://doi.org/10.1061/JBENF2.BEENG-5978

Damage localization in a steel truss bridge using influence lines identified from vehicle-induced acceleration

Said Quqa[a,*] and Luca Landi[a]

[a] *Department DICAM, University of Bologna, Viale del Risorgimento 2, 40136 Bologna, Italy*

ABSTRACT

In the last few decades, structural health monitoring (SHM) has proven a helpful tool to support the maintenance and management of civil infrastructure. However, typical measurement networks are expensive and require considerable initial efforts. The user-friendliness and interpretability of the outcome of SHM systems is a crucial factor in motivating infrastructure owners and decision-makers to sustain their costs. For this reason, simple algorithms that provide structural parameters with direct physical interpretability for professionals familiar with the typical quantities involved in structural engineering are still the most used in field applications. This paper proposes an original method to identify curvature influence lines of bridges and viaducts only using the structural acceleration response induced by vehicular loads. Acceleration time histories collected at sparse locations through standard accelerometers are employed. In contrast to SHM approaches based on modal parameters, the proposed method does not need strict synchronization, thus being suitable for wireless and low-cost monitoring solutions. Identified influence lines are used to define a spatially-dense damage indicator for accurate localization of structural anomalies with a clear physical meaning. Experimental results obtained for a steel truss bridge analyzed in different damage conditions prove the efficacy of the proposed method also for situations where modal-based approaches may fail.

KEYWORDS: damage identification, structural health monitoring, steel bridge, curvature, influence line, accelerometer.

Declaration of interests: The authors declare that they have no known competing financial interests or personal relationships that could have appeared to influence the work reported in this paper.

---

* Correspondence to: Said Quqa, Department DICAM, University of Bologna, Viale Risorgimento 2, 40136 Bologna, Italy, e-mail: said.quqa2@unibo.it

E-mail addresses: said.quqa2@unibo.it (S. Quqa), l.landi@unibo.it (L. Landi).

1. INTRODUCTION

Developed economies depend on complex and capillary transportation infrastructure that guarantees economic exchange and allows the transportation of people and goods. In the last decades, the implementations of structural health monitoring (SHM) systems in civil infrastructure have rapidly grown to inform owners of viaducts and galleries of their structural conditions, thereby supporting maintenance and management operations.

Traffic is the primary excitation source for road infrastructure and typically induces significant vibration to the structural components. While, in the last decades, operational modal analysis (OMA) for vibration-based SHM has mainly focused on ambient vibration data (Aloisio et al. 2020c; Brincker and Ventura 2015), recent studies have demonstrated that traffic-induced response may enclose valuable information on the structural behavior. For instance, Aloisio et al. (2020a) used traffic vibration to identify the elastic moduli of reinforced concrete (RC) viaducts. Also, Aloisio et al. (2022) highlighted the importance of moving loads to identify structural parameters of railway bridges related to track-ballast-bridge interaction. Khan et al. (2021) used the structural response to vehicular loads to identify damage related to scour. Furthermore, traffic excitation increases vibration amplitude, thus facilitating data collection with relatively low-cost sensing systems (e.g., microelectromechanical systems, MEMS) with a higher noise floor compared to more "traditional" piezoelectric devices (Sabato et al. 2017).

Due to the ability of traditional sensing systems to collect only the medium-high frequency range of vibration, the first (and still most popular) SHM systems rely on modal parameters (Aloisio et al. 2020b; Bhowmik et al. 2020; Lynch et al. 2006; Sabato et al. 2017; Tronci et al. 2022). However, mode shapes identified using sparse accelerometers are only evaluated at the instrumented locations. Dense sensor networks are thereby necessary for accurate damage localization (Quqa et al. 2022b). Besides, time synchronization between different sensing nodes is typically required to correctly identify the phase information used to determine the sign of mode shapes. In addition, SHM approaches based on traffic-induced vibration typically use long time histories to satisfy the assumption of stationary input at the base of most identification algorithms (Brincker and Ventura 2015). Together with the data synchronization needs, this aspect may considerably increase the cost of sensor networks, as they require a constant power supply and cables or other synchronization strategies to set a common time reference.

Although sensing technologies have evolved rapidly, modal parameters and derived quantities, such as modal flexibility (Toksoy and Aktan 1994) and curvature (Zhang and Aktan 1998), are still the most used damage-sensitive features (DSFs) in SHM due to their intuitive physical interpretation (Lynch et al. 2006; Sabato et al. 2017). In particular, modal curvature has always been one of the most effective damage indicators to identify local stiffness reductions in structural components (Dessi and Camerlengo 2015; Fan and Qiao 2011). However, computing curvature from modal parameters introduces inaccuracies due to the sparsity of modal estimates that may amplify the effects of noise (Giordano and Limongelli 2020; Wu and Law 2004).

As an alternative to modal parameters, recent studies exploited the spatial information related to passing vehicles to identify dense structural features (Zheng et al. 2019). The structural response measured under vehicular loads can be processed to identify the influence lines of a bridge, representing the variation of a given effect (typically in terms of strain or displacement) in a structural member due to a moving load, as a function of its location.

Zaurin and Catbas (2011) integrated synchronized computer vision data and different sensor measurements (tiltmeters and strain gages) to identify rotation and strain influence lines during the passage of vehicles on instrumented bridges. Cavadas et al. (2013) proposed a data-driven method to detect and localize structural damage by analyzing the quasi-static displacement collected during the passage of a vehicle. The authors used moving principal component analysis (MPCA) and robust regression analysis (RRA), showing that combining these two methods provides relevant information on structural conditions. Chen et al. (2015) used train-induced strain data to identify the stress influence lines of structural elements through regularization approaches, which proved effective for localizing single and multiple damages of a suspension bridge. Frøseth et al. (2017) identified the strain influence lines of a railway bridge from sparse measurements collected under train excitation using deconvolution and stabilizing filters. He et al. (2017) proposed a damage quantification method based on influence lines identified from displacement measures of beam structures subjected to loads moving with low speed (i.e., below 1 m/s) to suppress the dynamic component in the collected dataset. Wang et al. (2017) identified strain and displacement influence lines by fitting the structural response to piecewise polynomials and harmonic sinusoids, which model the quasi-static and dynamic parts of the structural response, respectively. Chen et al. (2018b) presented a damage quantification method based on displacement influence lines obtained from prior knowledge of the stiffness or flexibility matrix of the monitored structure, which can be modeled using a numerical model and calibrated on field data. Wu et al. (2018) identified damage in a continuous concrete girder bridge by analyzing the areas of influence lines obtained from data collected through distributed long fiber Bragg grating (FBG) strain sensors. Heitner et al. (2020) presented an iterative method to identify the strain influence line and the relative axle weights of passing vehicles. Moreover, the authors proposed the concept of "population influence line" as an elegant and robust synthesis of the bridge behavior under different loading patterns. Martinez et al. (2020) used a similar iterative approach to determine the displacement influence line and the axle weight of vehicles in random traffic conditions. Breccolotti and Natalicchi (2022) used displacement and rotation measurements, as well as WIM data to identify displacement influence lines and the local stiffness of bridges with different geometrical schemes. The authors tested the method using numerical simulations, obtaining promising results.

All the mentioned studies use strain or displacement data to identify influence lines. However, several researchers (Alamdari et al. 2019; OBrien et al. 2021a) found that the success of strain-based methods strongly depends on the closeness of damage to the sensor location. Therefore, several strain gauges may be necessary to identify damage correctly. On the other hand, displacement sensors, such as laser doppler vibrometers (LDVs) and linear variable differential transducers (LVDTs), are typically expensive and need a fixed reference, which is hard to find in long-term field applications (Nassif et al. 2005).

Recently, Martini et al. (2022) used multiple cameras to identify vehicle loads, their location on the bridge, and the structural displacement at target positions. Dealing with camera recordings may be particularly challenging due to their sensitivity to light conditions and disturbing objects. Avoiding strain and displacement measurements, Alamdari et al. (2019) proposed a method to identify rotation influence lines considering only two instrumented locations at the bridge bearings. They used this feature to assess cable losses in a cable-stayed bridge. Huseynov et al. (2020) used accelerometers to retrieve structural rotation and the relevant influence lines for damage identification in terms of loss in the bending stiffness of the bridge deck. The authors also found that, for simply supported bridges, the optimal sensor setup involves two sensors at the supports. A few years later, O'Brien et al. (2021) used rotation measurements collected through a bridge weigh-in-motion (B-WIM) system for damage identification, observing that when damage occurs, the rotation-based B-WIM system overestimates vehicle weights. Also, O'Brien et al. (2021b) obtained acceleration influence lines for damage detection using an iterative approach without the need for pre-weighing of vehicles. The authors showed that a local loss of stiffness at any bridge location could affect bridge accelerations at every physical point. However, localization and quantification of damage need further studies.

Accelerometers are still the most used sensing solutions for vibration-based SHM due to the simplicity of use and the availability of a wide set of commercial devices with different technical specifics and costs, allowing tailored solutions for different case studies. However, several challenges undermine the direct use of acceleration data to identify influence lines. First, all measurement amplitudes – including strain and displacements – depend on the vehicle weight (OBrien et al. 2021b), which is not typically measured in SHM applications. Nevertheless, this last aspect can be accounted for relatively easily by using WIM systems, which are becoming increasingly accurate lately (Chen et al. 2018a; He et al. 2019; Huseynov et al. 2022; Sekiya et al. 2018). However, one of the most important aspects that differentiate strain or displacement measurements from acceleration data is that, in the case of acceleration data, the measurement amplitude also depends on the vehicle speed and its variations.

Quqa et al. (2021) recently proposed a method to obtain curvature influence lines from acceleration data through simple low-pass filters. The results showed a relatively high variance of the identified features depending on the vehicle speed and path. A similar filtering approach with bandpass filters was also applied to the same acceleration signals to identify modal parameters (Quqa et al. 2020). Although leading to more robust estimates, their sparsity would not allow accurate localization of curvature variations. In another paper, Quqa et al. (2022a) showed that a unified monitoring approach based on a filter bank made of both low-pass and bandpass filters can be used to identify different structural features in a computationally convenient fashion exploiting analog in-memory computing technology.

This paper presents the first experimental results obtained for damage localization using only influence lines identified from acceleration data collected on a real case study with artificially induced damage. Compared to the proof-of-concept presented by (Quqa et al. 2021), this study removes the influence line normalization, which hindered the localization of anomalies close to the instrumented location. A control parameter is introduced instead, based on the area of the identified feature, and employed to remove outliers generated by anomalous vehicle speeds or masses, which may affect identification accuracy. Moreover, this study calculates the damage index by exploiting the superposition principle, considering all the sensors deployed on the structure and improving robustness in damage localization. The method proposed in this paper is based on the following assumptions:

1) One single vehicle is traveling the monitored bridge span,
2) The vehicle has an approximately constant speed,
3) Dynamic vehicle-bridge interaction is neglected,
4) The frequency range of measurement goes down to 0 (i.e., direct current – DC).

The first two assumptions can be realistic in the case of relatively small bridges with simply supported decks and fluid traffic conditions. The third assumption can be considered valid since the proposed procedure only accounts for the quasi-static part of the structural response, filtering out all signal components higher than about 1 Hz. The last assumption is respected if particular accelerometers (e.g., MEMS or force balance) are employed.

The main advantage of the proposed method compared to "traditional" approaches, e.g., based on modal parameters, is that the influence line obtained at a given location carries dense spatial information of the entire structure. Therefore, by analyzing local variations in the identified features, damage localization can be achieved using sparse sensors, which do not need strict time synchronization and can operate almost individually.

In this paper, Section 2 presents the outline of the algorithm for identifying influence lines and calculating a dense damage indicator from sparse acceleration time histories. Section 3 presents the experimental results obtained for the Old ADA Bridge (Japan), tested with artificially induced damage scenarios. Section 4 reports the main concluding remarks of the study.

2. PROCEDURE OUTLINE

2.1 Identification of curvature influence lines

Consider a simply-supported beam subjected to a concentrated load P moving with a constant speed v along the axis of the structure. This dynamic system can be described using the following equation:

$$\mu \frac{\partial^2 u(z,t)}{\partial t^2} + d \frac{\partial u(z,t)}{\partial t} + EI \frac{\partial^4 u(z,t)}{\partial z^4} = P\delta(z - vt) \tag{1}$$

where $u(z,t)$ is the structural displacement, z and t are the space and time variables, μ is the mass per unit length of the beam, d is the damping coefficient, and EI is the flexural stiffness of the beam, given by the elastic modulus of the material E and the inertia of the section I. In Eq. (1), δ represents a Dirac delta function. The solution to Eq. (1) consists of a dynamic and a quasi-static components, as shown in (Quqa et al. 2021). Specifically, the latter component represents the displacement of the beam in z obtained by applying a static load at the (moving) location $\hat{z} = vt$.

Since $\hat{z}$ spans the entire beam at the passage of a vehicle, the quasi-static structural response in z can be interpreted as the displacement influence line of the beam calculated in the reference section z. A more detailed description of the quasi-static component of the structural response and the related equations can be found in (Quqa et al. 2021) and are not reported here for brevity.

Assuming the total length of the beam equal to l, consider an accelerometer installed at a section distant ζl from the first support (with $\zeta \in [0,1]$) collecting the structural response in this location with a given sampling frequency F_s. It is worth noting that, in this case, the measure is available only at discrete values of time (and thus, of $\hat{z}$). The collected response consists of a dynamic and a quasi-static component, represented by the double derivatives of the displacement counterparts mentioned above. Since the quasi-static component does not include dynamic effects, and the dependence of time only determines the location of the applied load, its double derivative over time is proportional to its double derivative over $\hat{z}$. Therefore, the quasi-static part of the acceleration response represents the influence line of the curvature of the beam computed in the instrumented location and can be calculated as (Frýba 1999; Quqa et al. 2021):

$$h^{(\zeta)}[\hat{z}] \approx -\frac{Pl^3}{48EI}\sum_{m=1}^{\infty}\frac{\pi^2 v^2 \sin(m\pi\zeta)}{l^2(m^2-\alpha^2)}\sin\left(\frac{m\pi\hat{z}}{l}\right) \tag{2}$$

with

$$\alpha = \frac{vl}{\pi}\sqrt{\frac{\mu}{EI}} \tag{3}$$

Quqa et al. (2021) also demonstrated that $h^{(\zeta)}[\hat{z}]$ is non-negligible only for the first few terms of the summation reported in Eq. (2). Therefore, the frequency spectrum of $h^{(\zeta)}[\hat{z}]$ is significant only in the low-frequency range. On the other hand, if damping is low, the dynamic effects of the structural response are significant only in the proximity of the resonant frequencies of the system, the first of which are generally in the order of a few hertz for ordinary RC and steel simply supported bridge decks. For this reason, processing the raw acceleration collected during the passage of moving loads (i.e., vehicles) through a low-pass filter is generally enough to isolate the quasi-static part of the structural response. In this case, the curvature influence line can be calculated from the structural acceleration response as:

$$h^{(\zeta)}[\hat{z}] = \left(\left. \frac{\partial^2 u(z,t)}{\partial t^2} \right|_{z=\zeta l,\ t=\hat{z}/v} * \bar{b}_0 \right) [\hat{z}] \tag{4}$$

where $*$ is the convolution operator, $\bar{b}_0[\tau]$ is the impulse response of a low-pass filter with cutoff frequency below the first resonant frequency of the monitored structure, and τ is the tap index of the filter. More details on suitable low-pass filters are provided in Section 3.

In this study, passing vehicles are assumed as moving loads. Although real vehicles have two or more wheel axles and thus can be more accurately modeled using multiple applied forces, a previous study demonstrated that the single-load simplification does not involve significant differences at low frequencies if the span length is in the order of 10 times the distance between the axles of the considered vehicles (Quqa et al. 2021).

Since only the quasi-static part of the structural response is processed in this algorithm, suitable sensors that collect vibration at low frequencies (i.e., DC) should be employed. For instance, MEMS and force balance accelerometers (FBAs) generally satisfy this condition. Moreover, lower sampling frequencies can be set compared to traditional systems employed to identify modal parameters since, in this case, the sampling frequency only dictates the discretization rate of $\hat{z}$. Furthermore, as each sensor is used to identify an individual influence line, strict time synchronization between accelerometers is unnecessary.

Quasi-static features identified through low-pass filtering from raw acceleration should be cautiously interpreted. Bias, drift, and flicker noise can populate the low-frequency range of the acceleration response (Djurić 2000). These phenomena are mainly due to instrumentation noise and the effects of road roughness. Herein, a method is proposed to remove a linear trend from the identified influence lines to mitigate drifts in the identified features. Specifically, since the beam curvature at the instrumented location should be zero when the load is at the supports, a linear estimate of the bias and drift that may affect the identified influence line can be calculated as the reference line:

$$r^{(\zeta)}[\hat{z}] = h^{(\zeta)}[0] + \frac{h^{(\zeta)}[L] - h^{(\zeta)}[0]}{L}\hat{z} \tag{5}$$

where $h^{(\zeta)}[0]$ and $h^{(\zeta)}[L]$ indicate the elements of the identified influence line at the instants when the load is on the first and last support, respectively. In order to mitigate the effects of bias and drift, the estimated reference can be subtracted from the identified influence line as:

$$\bar{h}^{(\zeta)}[\hat{z}] = h^{(\zeta)}[\hat{z}] - r^{(\zeta)}[\hat{z}] \tag{6}$$

Moreover, other noise effects can be mitigated by averaging the influence lines identified for different vehicles. Since different vehicles may have different speeds, $\bar{h}^{(\zeta)}[\hat{z}]$ generally has a variable length, thus not allowing a direct average. Therefore, each realigned influence line should be first interpolated to a grid of fixed locations and then averaged to provide a more robust curvature estimate at the grid points (e.g., using spline interpolation (Quqa et al. 2021)).

A general identification algorithm for a single estimate of the curvature influence line (called "sample" hereafter) is thus schematized in Fig. 1 and can be summarized as:

1) Collect the acceleration time history at a given instrumented location and apply the low-pass filter,
2) Cut the filtered signal at the instants where the load enters and leaves the monitored bridge span,
3) Subtract the reference line from the obtained estimate,
4) Interpolate the curvature values to a fixed grid.

If the structure is statically determined, the curvature influence line computed in a given section ζ can also be interpreted as the curvature diagram of the structure (which is also proportional to the bending moment diagram) obtained by applying a static load in ζ. As previously mentioned, the curvature is one of the most used DSFs for SHM, which typically increases in damaged intervals (Dessi and Camerlengo 2015). Therefore, supposing to identify an average influence line (using several samples) at the beginning of the monitoring process (namely, the "baseline" condition) and at periodic intervals (namely, the "inspection" conditions), the difference between the average inspection and baseline estimates can be effectively employed as a damage indicator. This difference will be referred to as "difference function" for simplicity.

Previous results (Quqa et al. 2021) showed that, for simply-supported beams, clear peaks appear in the difference function obtained from inspection and baseline influence lines normalized to their maximum values at the locations where the flexural stiffness was locally reduced. Moreover, due to normalization, the peak magnitudes were also representative of the damage entity (assuming particular constraints on the vehicle speed). This approach has shown to be particularly effective if the damage was not in the proximity of the instrumented location. On the other hand, if the damage was close to a sensor, the maximum value of the inspection influence line was in the damaged portion. Therefore, due to data normalization, the difference function was close to zero in the damaged interval, making the determination of peaks particularly challenging. In truss bridges, sensors are typically deployed at the nodes of the structure, which are locations prone to damage. In this study, a different definition of the damage index is proposed, avoiding the normalization of identified influence lines and thus providing accurate localization of the structural damage even if the anomaly is close to the instrumented locations.

2.2 Definition of a damage indicator based on the superposition principle

Assuming a linear-elastic structural behavior during the passage of regular vehicles, the superposition principle can be exploited to calculate the curvature diagram of the structure subjected to a set of uniform concentrated loads applied at all the instrumented locations. This diagram is obtained by summing the influence lines identified at all the instrumented sections. A damage indicator is then defined as the difference of the curvature diagrams thus obtained:

$$D[\hat{z}] = \sum_{i=1}^{r} \bar{h}_d{}^{(\zeta_i)}[\hat{z}] - \sum_{i=1}^{r} \bar{h}_b{}^{(\zeta_i)}[\hat{z}] \tag{7}$$

In Eq. (7), $\bar{h}_d{}^{(\zeta_i)}[\hat{z}]$ and $\bar{h}_b{}^{(\zeta_i)}[\hat{z}]$ denote the average influence lines identified at the i-th instrumented section for the inspection and baseline conditions, respectively, while r is the total number of instrumented locations.

Therefore, $D[\hat{z}]$ represents the increment in the curvature of the structure subjected to a uniform set of concentrated loads and is defined at all the values of $\hat{z}$ regardless of the number of instrumented locations. This approach is similar to the case of damage identification using the curvature of the uniform load surface (or line, in two-dimensional cases) (Quqa et al. 2020; Wu and Law 2004; Zhang and Aktan 1998) obtained by multiplying the flexibility matrix of the structure (calculated from identified modal parameters) with a uniform load vector. However, the proposed approach has two main advantages over the mentioned method:

1) Derivation errors introduced by typical methods employed to calculate curvature from sparse modal estimates (e.g., the central difference approximation (Giordano and Limongelli 2020; Wu and Law 2004)) are avoided.
2) The DSF and the damage index are spatially dense and not available only at the instrumented locations.

However, features identified simply by using filtering operations also have criticalities. First, each influence line is identified by analyzing a short signal and can be affected by short-term phenomena (i.e., non-stationarities, such as wind or nearby traffic vibration) and slight variations in the speed of the passing cars. Moreover, some dynamic effects could be included in the filtered signal, both due to the imperfect filtering ability of employed filters (thus including signal components above the selected cutoff frequency) and low-frequency dynamic components in the structural response. However, all these phenomena have a different influence on each identified sample; thereby, averaging the influence lines identified at the passage of several vehicles mitigates the dynamic components.

To have a consistent averaging process, however, it is necessary that the individual influence lines are not substantially different from one another, especially in terms of amplitude. The amplitude of influence lines mainly depends on vehicle mass and speed. Considering only vehicles within a given speed and mass range would thus produce similar influence lines. While speed can be easily calculated from the length of each sample, vehicle weight could be determined using B-WIM systems, which are becoming very popular for characterizing traffic load (Chen et al. 2018a; He et al. 2019; Huseynov et al. 2022; Sekiya et al. 2018), or roughly estimated using regular traffic cameras from the vehicle size or model. Upon selecting influence lines generated by a limited set of similar vehicles, anomalous estimates (e.g., due to non-constant speed) can be further removed by discarding the samples with an outlier area in a considered time window.

At the passage of each vehicle, the area of $\bar{h}^{(\zeta)}[\hat{z}]$ is calculated at each instrumented location. The influence line generally has an amplitude (and an area) that depends on the reference section (i.e., the instrumented location). An amplification factor can be calculated to make the areas of influence lines comparable based on the relevant instrumented locations. For instance, if the stiffness of the beam is almost constant, the amplification factor can be calculated as the ratio of the areas of the bending moment diagrams $M^{(\zeta)}(z)$ obtained by applying the load in $l/2$ and ζl:

$$\alpha^{(\zeta)} = \frac{\int_0^l M^{(0.5)}(z)dz}{\int_0^l M^{(\zeta)}(z)dz} = \frac{1}{4\zeta(1-\zeta)} \tag{8}$$

The amplified area of the curvature diagram can thus be calculated as:

$$A^{(\zeta)} = \alpha^{(\zeta)} \sum_{\hat{z}=0}^{L} \bar{h}^{(\zeta)}[\hat{z}] \tag{9}$$

It is worth noting that, given a vehicle weight, $A^{(\zeta)}$ should be constant for every ζ.

In this way, after forming a set S of $\bar{h}^{(\zeta)}$ estimates, only the ones with an amplified area $A^{(\zeta)}$ included in the range $[\mu_S - \beta\sigma_S, \mu_S + \beta\sigma_S]$ can be averaged to obtain the final estimate, where μ_S and σ_S are the mean and standard deviation of the amplified areas of the samples included in the set S, while β is a parameter that can be tuned to select the estimates with a user-defined variability for the final computation of the damage index. Considering samples calculated at different instrumented locations in the same set S is necessary to guarantee that the vehicle speed is uniform.

3. EXPERIMENTAL RESULTS

This section briefly describes the experimental case study and then reports the damage identification results using the proposed approach. The acceleration data for the case study (the Old ADA Bridge) is freely available online (Kim et al. 2021b) and described in (Kim et al. 2021a).

3.1 Case study

The Old ADA Bridge was a simply supported steel Warren-truss bridge with a main span length of 59.2 m and a width of 3.6 m. The bridge was built in 1959 and demolished in 2012 in Japan. A scheme of the case study with the general dimensions is illustrated in Fig. 2. More details can be found in (Kim et al. 2021a).

Before demolition, an experimental campaign was conducted to collect ambient and vehicle-induced vibration data. Five damage scenarios were artificially induced during the tests while blocking the traffic and using a single test vehicle. The vehicle was a Nissan Serena having a total weight of about 21 kN, including passengers and measurement devices. The spacing between the front and back wheel axles was 2.7 m, and the track width was 1.5 m. The first dominant frequency of the sprung motion of the vehicle body was identified at 1.7–1.8 Hz, while the first resonant frequency of the bridge was 2.98 Hz.

Four damage scenarios were artificially induced during the experimental campaign, as reported in Tab. 1. In this study, condition “U” represents the “undamaged” baseline configuration of the structure. In condition “DC1”, the cross-section of the vertical truss T1 at the bridge midspan (see Fig. 2) was cut to half and completely cut in condition “DC2”. The central truss was then repaired by lifting the bridge to the original height using a jack and soldering the damaged element ("DC3"). In this case, however, the bridge was not guaranteed to be restored to its original state. After recovering the first damaged truss, a second vertical truss (T2 in Fig. 2) was completely cut in condition "DC4".

It is worth noting that, although the section reductions may seem considerable, DC1 and DC3 can still be considered minor damage, as the element T1 is almost unloaded due to the particular geometry of the truss structure. Moreover, in DC3, the material continuity was fully restored. Indeed, (Chang and Kim 2016) noted that identification methods based on modal parameters could hardly identify damage in this condition.

In each condition, an ambient vibration test was carried out first, during which the structural vibration was collected without vehicle excitation. These tests were followed by vehicle-induced vibration tests, in which the acceleration response of the structure was acquired while passing with the test vehicle.

Eight uniaxial accelerometers were deployed on the bridge deck, as shown in Fig. 2, five on the side of the damaged truss member and three on the opposite side, collecting the acceleration in the vertical direction. The accelerometer model was "ARS-A" by Tokyo Measuring Instruments, with a nominal responding frequency from DC to 30 Hz. Besides these, two optical sensors ("PZ-G52" by Keyence Co.) were installed on the two ends of the bridge and one at the midspan to track the time instants when the vehicle passed in these three instrumented locations. All sensors were connected to data loggers, guaranteeing time synchronization. All the time histories were sampled at 200 Hz. During the tests, no substantial temperature change was observed.

3.2 Discussion

In this study, ten acceleration time histories collected during the passage of the test vehicle at about 40 km/h (herein called "samples") are used to calculate the curvature influence lines of the bridge deck.

The low-frequency component of each sample is extracted using a low-pass wavelet filter. Specifically, the reverse biorthogonal filter with three vanishing moments has proved very selective in a previous study (Quqa et al. 2022a). Moreover, the modest number of taps of the impulse response of the mentioned filter makes computations particularly efficient and thus suitable also for battery-powered sensing nodes. The wavelet filter was obtained by cascading eight low-pass *rbio3.1* filters, each with a dyadic upsampling with respect to the previous one, thus resulting in a wavelet transform of level $n = 8$ (Vetterli and Kovačević 1995). The theoretical cutoff frequency of the resulting filter, calculated as $f_{cutoff} = F_s/2^{n+1}$ is thus 0.39 Hz (Quqa et al. 2021; Vetterli and Kovačević 1995). Fig. 3 shows the response spectra of the acceleration collected at location A2 during the passage of a single car, the low-pass wavelet filter obtained as described above, and the related filtered response. It is possible to observe that the filtering operation mitigates the resonant peaks of the structural response related to the dynamic effects, and only the quasi-static component below the cutoff frequency has a significant amplitude.

A total of 10 influence lines were identified by applying the algorithm described in Section 2.1 for each instrumented location and damage condition, thus collecting and analyzing the data for 50 different passages of the test vehicle. The left-hand side of Fig. 4 shows the influence lines identified for each recording, together with their average, organized in different plots for each damage scenario. The average influence lines are computed after discarding the estimates with a sample area outside the boundaries described in Section 2. Here, the parameter β was set equal to

2, thus assuming to use the 95% of collected samples if their amplified areas are normally distributed. The left-hand part of the figure reports the amplified areas obtained using Eq. (8) for all instrumented locations. The sample means and standard deviations of these areas are reported in Tab. 2. Since the test car is always the same, the amplified areas are almost constant. From the values shown in the table, it is possible to notice that, in general, the areas of the damaged conditions are slightly higher compared to those of the baseline, denoting a higher total curvature of the bridge deck. Moreover, excluding the outliers, the mean area of DC4 is lower than that of DC2 and DC3, representing the restoring intervention. However, a clear correlation of the total curvature with the damage entity is not observable in terms of global curvature since DC2 and DC3 have a similar area, although the damage in DC3 is more severe.

The damage index proposed in Section 2.2 was calculated considering two different sensor setups, i.e., (a) employing all five sensors on one side of the bridge from A1 to A5 and (b) only the two external sensors, A1 and A5. The spatial distribution of this index in the two mentioned situations is reported in Fig. 5(a) and 5(b), respectively.

Due to the modest number of samples considered in this application (i.e., 10 per damage condition), the average influence line, and thus the damage indicator, is still affected by local disturbances, such as the oscillations due to residual dynamic effects. Dashed lines represent the damage index obtained after the average process in Fig. 5(a-b). In order to consider a more extensive averaging process over a larger set of samples, Fig. 5(a-b) also reports the moving average of the damage index considering a kernel length of 40 elements. This “cleaned” diagram is represented using solid lines.

The curvature increment is observable throughout the beam length. However, the maximum curvature variations (highlighted by arrows) are always close to the locations of the damaged elements, even in the case of sparse sensor setup. It is worth noting that the results obtained in the two sensor setups are comparable. State-of-the-art studies are generally based on two or more displacement sensors, dense systems of strain gauges, or vision-based methods capable of identifying features at all physical points of the structures using images. Here, in the sparse configuration, only two uniaxial accelerometers were used to localize damage at nodes, which do not coincide with the instrumented ones.

The damage indicator proposed in this paper should be carefully interpreted considering the structural scheme, especially for truss structures. Indeed, while stiffness reductions in structures with a constant cross-section would generate a local peak in $D[\hat{z}]$ in the proximity of the stiffness loss, damaged elements in truss structures may generate complex patterns of curvature variations.

A simple 2D finite element model (FEM) of the case study (schematized in Figure 6) is used to validate the experimental damage index. In this model, the steel system was assumed as a truss structure, with the element having the dimensions described in (Kim et al. 2021a). The bridge deck was modeled as a continuous beam with a cross-section of 0.5×8.0 m. No calibration was conducted, as the aim of the comparison is only qualitative. The theoretical curvature difference of the bridge deck loaded with a set of uniform concentrated forces obtained by simulating a section reduction in T1 and T2 through the FEM is reported in Fig. 5(c), normalized to the maximum value.

It is possible to observe that the experimental damage indicator in conditions DC1, DC2, and DC3 (Fig. 5(a-b)) has nearly symmetric distributions with a central peak, which is compatible with the theoretical result shown in Fig. 5(c). As already noted for the areas of the identified influence lines (see Tab. 2), the curvature distribution in DC1 and DC2 is almost coincident in Fig. 5(a), while DC2 has a lower magnitude in Fig. 5(b). While this fact may be justified considering a stress redistribution after DC1 and inelastic bridge settlement, the proposed method was not validated to estimate the damage entity at this stage. Nevertheless, the restoring process carried out between DC2 and DC3 leads to a curvature reduction for the latter condition. The curvature difference between conditions DC3 and U is still higher than zero, reflecting a residual effect of the damage induced in DC1 and DC2 that was not completely recovered. For both the dense and sparse sensor setups, the peak in curvature difference for DC4 is at the location of T2, thus reflecting the new damage and being consistent with the theoretical result reported in Fig 5(c).

Nevertheless, while the theoretical result has an almost constant curvature except for the interval between 296 and 444 cm, the experimental result shows higher curvature values throughout the beam. It is worth noting that the damage of T2 was induced starting from DC3, which already presents slight damage in T1. Therefore, DC4 can be seen as a combination of the two theoretical results shown in Fig 5(c). Indeed, in the intervals between 0 and 296 cm, as well as between 444 and 592 cm, DC3 and DC4 are almost coincident.

Chang and Kim (2016) applied different damage identification techniques based on modal parameters to the data collected on the ADA bridge. Comparing the results presented in this paper with those of the mentioned study, it is observable that, in general, the proposed approach has superior sensitivity to small damage (i.e., DC1 and DC3). Indeed, Chang and Kim (2016) observed that modal parameters (both natural frequencies and mode shapes) change slightly from U to DC1 and are almost unchanged between U and DC3. Kim et al. (2014) attributed the low sensitivity of modal parameters to damage to stress redistribution.

In (Chang and Kim 2016), outlier analyses were conducted considering different sets of identified modal parameters to assess their sensitivity to damage. Univariate analyses using a single identified mode frequency resulted in accurate damage identification only for conditions DC2 and DC4. Similarly, clear damage detection is achieved for the same conditions using the modal assurance criterion (MAC) on individual mode shapes. Damage is correctly detected in DC1 only when multivariate analyses are conducted considering multiple natural frequencies or coordinate MAC (COMAC) values. However, identifying high modes is typically challenging. Kim et al. (2014) observed that higher modes could only be identified from forced-vibration responses for the analyzed case study, which generally provide lower precision than the parameters identified in free vibration.

4. CONCLUSIONS

This paper proposed a new damage indicator based on curvature influence lines identified only from traffic-induced vibration. The influence lines are determined using individual time histories, thus not needing strict time synchronization between sensors – which is typically necessary to identify modal parameters. This damage-sensitive feature is spatially dense and insensitive to derivation inaccuracies introduced by the central difference approximation or similar approaches commonly used to calculate curvature from sparse modal estimates.

The damage indicator proposed in this study is representative of variations in the curvature diagram obtained by applying a set of uniform loads to the structure. Using the proposed approach with acceleration data collected on a steel truss bridge with damaged elements allowed for accurate damage localization. In the analyzed structure, the damage indicator showed clear peaks close to the damaged components, even in the case of sparse sensor network (i.e., using only two sensors). Due to the intuitive physical sense of the damage indicator, the damaged elements can be accurately identified by interpreting the results with the support of a simple structural model.

In the presented monitoring approach, moving vehicles act as concentrated loads applied to limited structural portions. This is why, compared to other techniques based on modal parameters, the proposed method has shown superior sensitivity to minor damage. Moreover, while modal-based approaches generally need to identify high modes to localize minor damage correctly, the proposed method only consists of filtering the low-frequency component of the structural response. This makes the algorithm simple and computationally effective, as filtering can be done as a convolution.

In real-life applications, dense sensor setups for vibration-based structural health monitoring are typically affected by data transmission problems and synchronization. The proposed method, involving few sensors operating individually, brings enormous benefits, also providing dense features for accurate localization of structural anomalies. Moreover, compared to typical controlled loading tests, the proposed approach is based merely on acceleration measurements, which can be collected with the bridge in operation without interrupting traffic or needing a fixed reference (necessary for displacement measurements). Traffic intensity (i.e., to understand when only one vehicle is traveling the bridge) and a rough estimate of vehicle weight can be easily obtained through one simple traffic camera. The proposed method is meant to be used with a wide set of measurements in a long-term monitoring process. Therefore, modest vehicle mass and speed variability would slightly affect the final averaged influence line used for damage identification.

DATA AVAILABILITY

The data used during this study are available online (https://doi.org/10.17632/sc8whx4pvm.2) in accordance with funder data retention policies.

ACKNOWLEDGEMENTS

The authors would like to gratefully acknowledge the availability of data recorded on the Old ADA Bridge, freely available at (Kim et al. 2021b).

REFERENCES

Alamdari, M. M., Kildashti, K., Samali, B., and Goudarzi, H. V. (2019). "Damage diagnosis in bridge structures using rotation influence line: Validation on a cable-stayed bridge." *Engineering Structures*, 185, 1–14.

Aloisio, A., Alaggio, R., and Fragiacomo, M. (2020a). "Time-domain identification of the elastic modulus of simply supported box girders under moving loads: Method and full-scale validation." *Engineering Structures*, 215.

Aloisio, A., Alaggio, R., and Fragiacomo, M. (2020b). "Dynamic identification and model updating of full-scale concrete box girders based on the experimental torsional response." *Construction and Building Materials*, 264.

Aloisio, A., Di Battista, L., Alaggio, R., and Fragiacomo, M. (2020c). "Sensitivity analysis of subspace-based damage indicators under changes in ambient excitation covariance, severity and location of damage." *Engineering Structures*, 208, 110235.

Aloisio, A., Rosso, M. M., and Alaggio, R. (2022). "Experimental and Analytical Investigation into the Effect of Ballasted Track on the Dynamic Response of Railway Bridges under Moving Loads." *Journal of Bridge Engineering*, 27(10).

Bhowmik, B., Tripura, T., Hazra, B., and Pakrashi, V. (2020). "Real time structural modal identification using recursive canonical correlation analysis and application towards online structural damage detection." *Journal of Sound and Vibration*, Elsevier Ltd, 468, 115101.

Breccolotti, M., and Natalicchi, M. (2022). "Bridge Damage Detection Through Combined Quasi-static Influence Lines and Weigh-in-motion Devices." *International Journal of Civil*

Engineering, 20(5), 487–500.

Brincker, R., and Ventura, C. E. (2015). *Introduction to Operational Modal Analysis*. *Introduction to Operational Modal Analysis*, John Wiley and Sons, Ltd.

Cavadas, F., Smith, I. F. C., and Figueiras, J. (2013). “Damage detection using data-driven methods applied to moving-load responses.” *Mechanical Systems and Signal Processing*, 39(1–2), 409–425.

Chang, K.-C., and Kim, C.-W. (2016). “Modal-parameter identification and vibration-based damage detection of a damaged steel truss bridge.” *Engineering Structures*, 122, 156–173.

Chen, S.-Z., Wu, G., Feng, D.-C., and Zhang, L. (2018a). “Development of a Bridge Weigh-in-Motion System Based on Long-Gauge Fiber Bragg Grating Sensors.” *Journal of Bridge Engineering*, 23(9).

Chen, Z.-W., Cai, Q.-L., and Zhu, S. (2018b). “Damage quantification of beam structures using deflection influence lines.” *Structural Control and Health Monitoring*, 25(11), e2242.

Chen, Z.-W., Zhu, S., Xu, Y.-L., Li, Q., and Cai, Q.-L. (2015). “Damage Detection in Long Suspension Bridges Using Stress Influence Lines.” *Journal of Bridge Engineering*, 20(3), 05014013.

Dessi, D., and Camerlengo, G. (2015). “Damage identification techniques via modal curvature analysis: Overview and comparison.” *Mechanical Systems and Signal Processing*, Elsevier, 52–53(1), 181–205.

Djurić, Z. (2000). “Mechanisms of noise sources in microelectromechanical systems.” *Microelectronics Reliability*, 40(6), 919–932.

Fan, W., and Qiao, P. (2011). “Vibration-based damage identification methods: A review and comparative study.” *Structural Health Monitoring*, 10(1), 83–111.

Frøseth, G. T., Rønnquist, A., Cantero, D., and Øiseth, O. (2017). “Influence line extraction by deconvolution in the frequency domain.” *Computers and Structures*, 189, 21–30.

Frýba, L. (1999). *Vibration of Solids and Structures under Moving Loads*. *Vibration of Solids and Structures under Moving Loads*, Springer Science & Business Media.

Giordano, P. F., and Limongelli, M. P. (2020). “Response-based time-invariant methods for damage localization on a concrete bridge.” *Structural Concrete*, 21(4), 1254–1271.

He, W., Ling, T., OBrien, E. J., and Deng, L. (2019). “Virtual Axle Method for Bridge Weigh-in-Motion Systems Requiring No Axle Detector.” *Journal of Bridge Engineering*, 24(9).

He, W. Y., Ren, W. X., and Zhu, S. (2017). “Damage detection of beam structures using quasi-static moving load induced displacement response.” *Engineering Structures*, 145, 70–82.

Heitner, B., Schoefs, F., OBrien, E. J., Žnidarič, A., and Yalamas, T. (2020). “Using the unit influence line of a bridge to track changes in its condition.” *Journal of Civil Structural Health Monitoring*, 10(4), 667–678.

Huseynov, F., Hester, D., OBrien, E. J., McGeown, C., Kim, C.-W., Chang, K., and Pakrashi, V. (2022). “Monitoring the Condition of Narrow Bridges Using Data from Rotation-Based and Strain-Based Bridge Weigh-in-Motion Systems.” *Journal of Bridge Engineering*, 27(7).

Huseynov, F., Kim, C., OBrien, E. J., Brownjohn, J. M. W., Hester, D., and Chang, K. . (2020). “Bridge damage detection using rotation measurements – Experimental validation.” *Mechanical Systems and Signal Processing*, 135, 106380.

Khan, M. A., McCrum, D. P., Prendergast, L. J., OBrien, E. J., Fitzgerald, P. C., and Kim, C. W. (2021). “Laboratory investigation of a bridge scour monitoring method using decentralized modal analysis.” *Structural Health Monitoring*, 20(6), 3327–3341.

Kim, C.-W., Zhang, F.-L., Chang, K.-C., McGetrick, P. J., and Goi, Y. (2021a). “Ambient and

Vehicle-Induced Vibration Data of a Steel Truss Bridge Subject to Artificial Damage." *Journal of Bridge Engineering*, 26(7), (ASCE)BE.1943-5592.0001730.

Kim, C.-W., Zhang, F., Chang, K.-C., McGetrick, P., and Goi, Y. (2021b). "Old_ADA_Bridge-damage_vibration_data." Mendeley Data, V2.

Kim, C., Chang, K., Kitauchi, S., McGetrick, P., Hashimoto, K., and Sugiura, K. (2014). "Changes in modal parameters of a steel truss bridge due to artificial damage." *Safety, Reliability, Risk and Life-Cycle Performance of Structures and Infrastructures*, CRC Press, 3725–3732.

Lynch, J. P., Wang, Y., Loh, K. J., Yi, J.-H., and Yun, C.-B. (2006). "Performance monitoring of the Geumdang Bridge using a dense network of high-resolution wireless sensors." *Smart Materials and Structures*, 15(6), 1561–1575.

Martinez, D., Malekjafarian, A., and OBrien, E. (2020). "Bridge health monitoring using deflection measurements under random traffic." *Structural Control and Health Monitoring*, 27(9).

Martini, A., Tronci, E. M., Feng, M. Q., and Leung, R. Y. (2022). "A computer vision-based method for bridge model updating using displacement influence lines." *Engineering Structures*, 259, 114129.

Nassif, H. H., Gindy, M., and Davis, J. (2005). "Comparison of laser Doppler vibrometer with contact sensors for monitoring bridge deflection and vibration." *NDT & E International*, 38(3), 213–218.

OBrien, E. J., Brownjohn, J. M. W., Hester, D., Huseynov, F., and Casero, M. (2021a). "Identifying damage on a bridge using rotation-based Bridge Weigh-In-Motion." *Journal of Civil Structural Health Monitoring*, 11(1), 175–188.

OBrien, E. J., McCrum, D., and Khan, M. A. (2021b). “Bridge damage detection using acceleration influence line calibrated without access to a pre-weighed vehicle.” *Bridge Maintenance, Safety, Management, Life-Cycle Sustainability and Innovations*, CRC Press, 1615–1620.

Quqa, S., Antolini, A., Franchi Scarselli, E., Gnudi, A., Lico, A., Carissimi, M., Pasotti, M., Canegallo, R., Landi, L., and Diotallevi, P. P. (2022a). “Phase change memories in smart sensing solutions for structural health monitoring.” *Journal of Computing in Civil Engineering*, 36(4), 04022013.

Quqa, S., Landi, L., and Diotallevi, P. P. (2021). “Automatic identification of dense damage-sensitive features in civil infrastructure using sparse sensor networks.” *Automation in Construction*, 128, 103740.

Quqa, S., Landi, L., and Diotallevi, P. P. (2022b). “Instantaneous identification of densely instrumented structures using line topology sensor networks.” *Structural Control and Health Monitoring*, 29(3).

Quqa, S., Landi, L., Paolo Diotallevi, P., and Diotallevi, P. P. (2020). “Instantaneous modal identification under varying structural characteristics: A decentralized algorithm.” *Mechanical Systems and Signal Processing*, Academic Press, 142, 106750.

Sabato, A., Niezrecki, C., and Fortino, G. (2017). “Wireless MEMS-Based Accelerometer Sensor Boards for Structural Vibration Monitoring: A Review.” *IEEE Sensors Journal*, 17(2), 226–235.

Sekiya, H., Kubota, K., and Miki, C. (2018). “Simplified Portable Bridge Weigh-in-Motion System Using Accelerometers.” *Journal of Bridge Engineering*, 23(1).

Toksoy, T., and Aktan, A. E. (1994). “Bridge-condition assessment by modal flexibility.”

Experimental Mechanics, 34(3), 271–278.

Tronci, E. M., De Angelis, M., Betti, R., and Altomare, V. (2022). "Multi-stage semi-automated methodology for modal parameters estimation adopting parametric system identification algorithms." *Mechanical Systems and Signal Processing*, 165, 108317.

Vetterli, M., and Kovačević, J. (1995). *Wavelets and Subband Coding*. *Book*, Prentice-hall.

Wang, N.-B., He, L.-X., Ren, W.-X., and Huang, T.-L. (2017). "Extraction of influence line through a fitting method from bridge dynamic response induced by a passing vehicle." *Engineering Structures*, 151, 648–664.

Wu, B., Wu, G., Yang, C., and He, Y. (2018). "Damage identification method for continuous girder bridges based on spatially-distributed long-gauge strain sensing under moving loads." *Mechanical Systems and Signal Processing*, 104, 415–435.

Wu, D., and Law, S. S. (2004). "Damage localization in plate structures from uniform load surface curvature." *Journal of Sound and Vibration*, 276(1–2), 227–244.

Yu, Y., Cai, C., and Deng, L. (2016). "State-of-the-art review on bridge weigh-in-motion technology." *Advances in Structural Engineering*, 19(9), 1514–1530.

Zaurin, R., and Necati Catbas, F. (2011). "Structural health monitoring using video stream, influence lines, and statistical analysis." *Structural Health Monitoring*, 10(3), 309–332.

Zhang, Z., and Aktan, A. E. (1998). "Application of Modal Flexibility and Its Derivatives in Structural Identification." *Research in Nondestructive Evaluation*, 10(1), 43–61.

Zheng, X., Yang, D. H., Yi, T. H., and Li, H. N. (2019). "Development of bridge influence line identification methods based on direct measurement data: A comprehensive review and comparison." *Engineering Structures*, 198.

Tables

Tab. 1 Description of damage conditions

Damage condition	Description
U	Baseline configuration
DC1	50% cross-section reduction of one truss in T1
DC2	100% cross-section reduction of one truss in T1
DC3	Recovered configuration
DC4	100% cross-section reduction in of one truss T2

Tab. 2 Statistical parameters of the amplified areas of curvature diagrams

Damage condition	Mean	Standard deviation	Mean excluding outliers
U	3.18	1.14	3.11
DC1	5.73	1.56	5.90
DC2	5.36	1.37	5.43
DC3	5.15	2.60	4.56
DC4	5.09	0.83	5.01

Figures

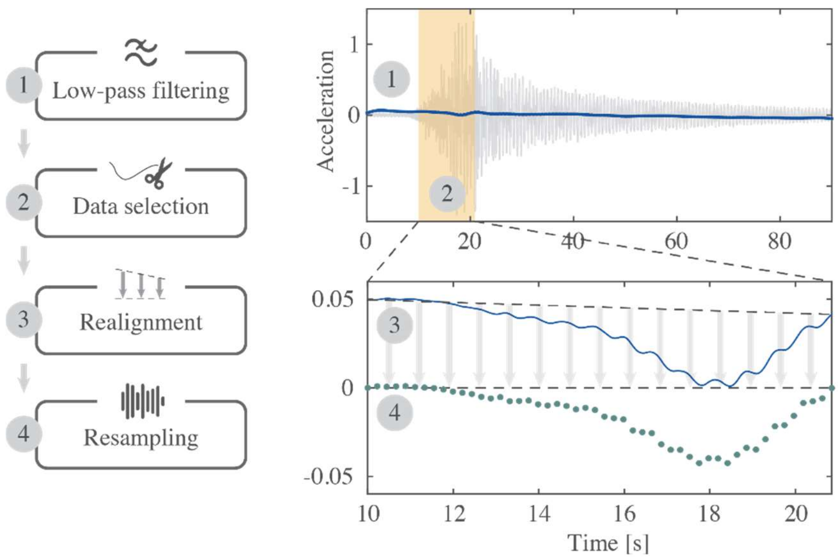

Fig. 1 – Scheme of the algorithm

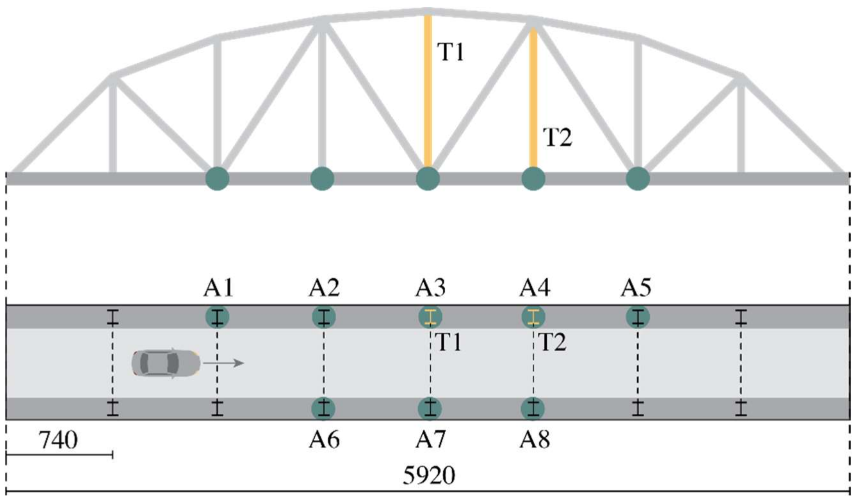

Fig. 2 – Scheme of the case study and sensor setup; dimensions in cm

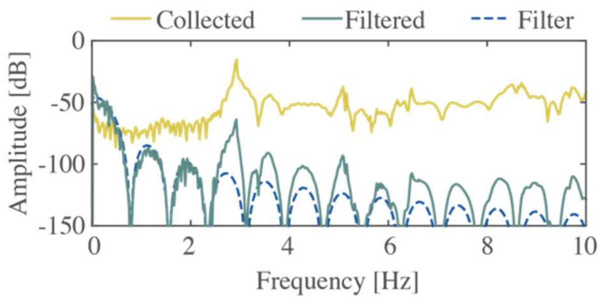

Fig. 3 – Frequency spectra of recorded time history, its filtered version, and the low-pass filter employed

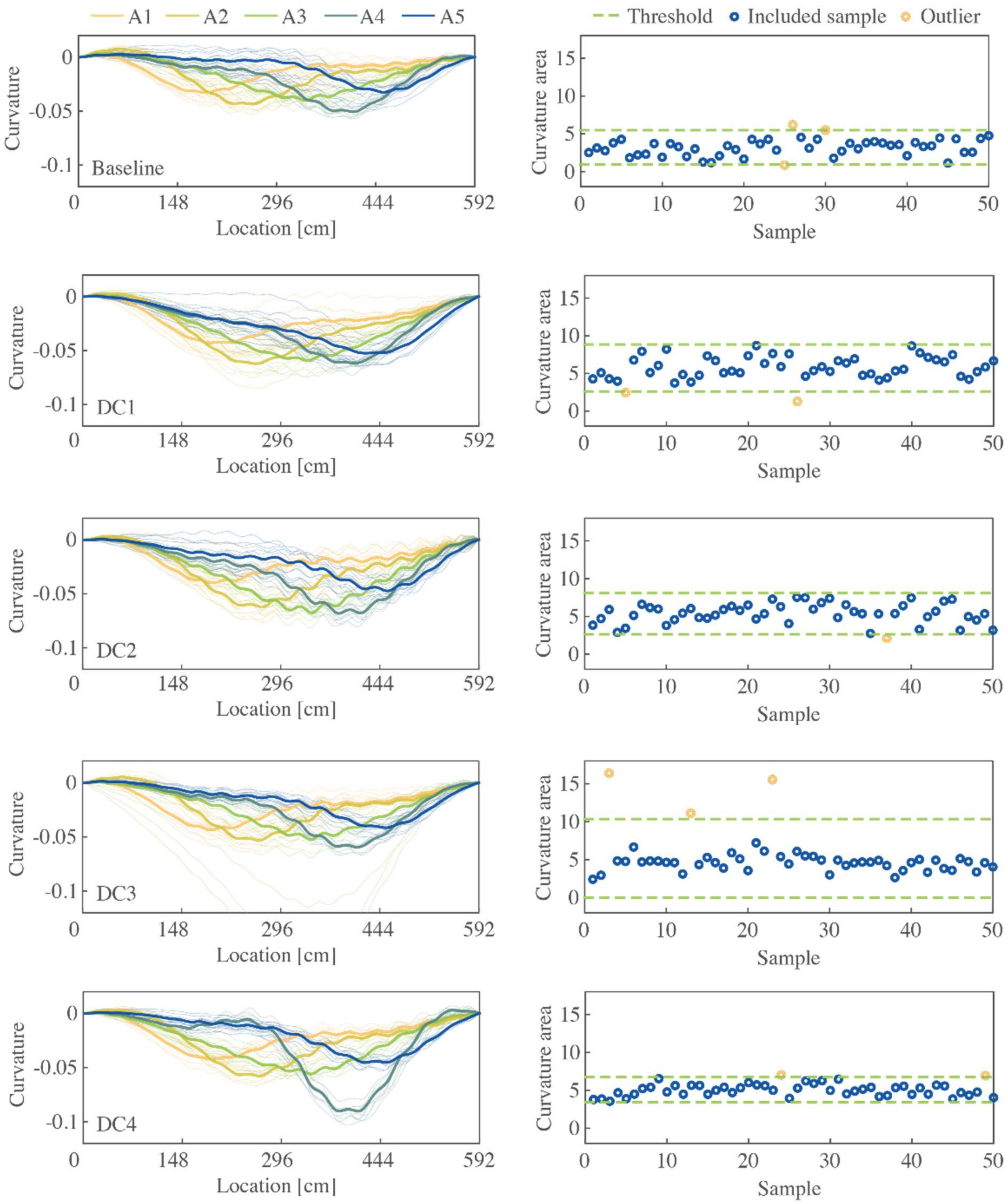

Fig. 4 – Identified influence lines (left) and amplified areas (right) calculated for each damage condition

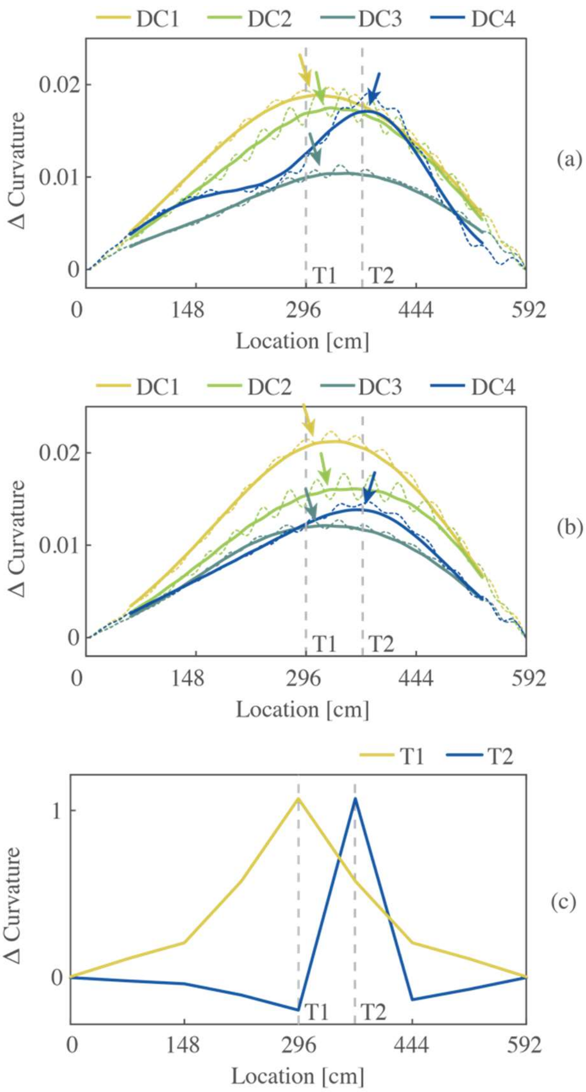

Fig. 5 – Difference of the total curvature diagrams obtained by applying uniform loads at the instrumented locations: (a) experimental results obtained using sensors A1-A5, (b) experimental results obtained using only sensors A1 and A5, and (c) results of the FEM

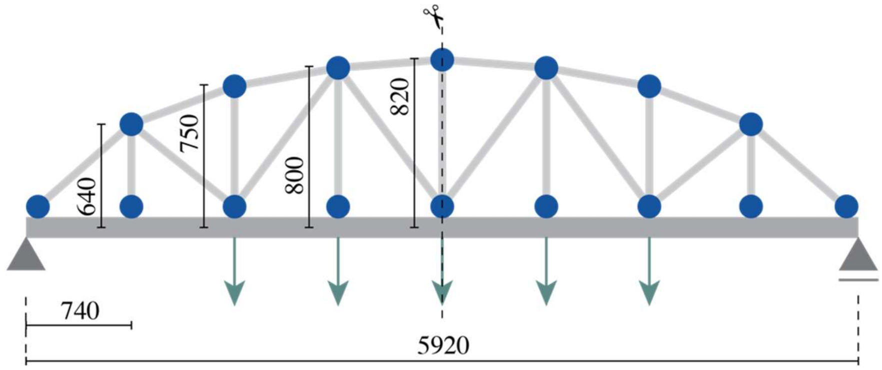

Fig. 6 – Scheme of the FEM and loads; dimensions in cm